Asynchronous Motor Test Bench for the Generation and Current Signal Diagnostics of Accelerated Bearing Damage

Christoph Anger[1], Christian Preusche[2], and Uwe Klingauf[3]

[1,2,3] *Institute of Flight Systems and Automatic Control, Technische Universität Darmstadt, Darmstadt, Hessen, 64287, Germany*
anger@fsr.tu-darmstadt.de
preusche@fsr.tu-darmstadt.de
klingauf@fsr.tu-darmstadt.de

ABSTRACT

The data acquisition of run to failure data by means of degrading components is one of the most delicate tasks in evaluating new diagnostic and prognostic approaches, since it is cost-intensive and time-consuming. Therefore, a test rig for a cost-efficient generation of artificial bearing damages is described below. The test rig is thereby based on an ordinary asynchronous motor.
This paper mainly concentrates on the description of the test rig's setup and first diagnostic findings. One aim of the experiments is the investigation of several variations of the applied loads for the artificially accelerated bearing aging. Thus, radial force and fluting are examined. The latter causes a damage triggered by a current flow through the test bearing. Both load types reduce the overall lifespan of bearings to about few weeks.
The generated faults are a broken cage and chattermarks due to a radial force higher than the design point. The bearings are diagnosed by means of frequency analysis of the phase current signal, which is produced in the stator of the motor. Beside the current signal, also temperature, vibration and revolution of the shaft are measured, whereas the vibration signal is used only for the comparison to the current signal. The comprehensive measurement concept allows a performance evaluation of diagnostic and prognostic algorithms based on different physical indicators.
It can be shown that especially the current frequency spectrum of a faulty bearing differs significantly from a healthy one. In order to face the high amount of measurement data, the Principal Component Analysis is used for data reduction to generate features for the diagnosis and prognosis. Thus, a classification of different fault modes and loading conditions is possible.

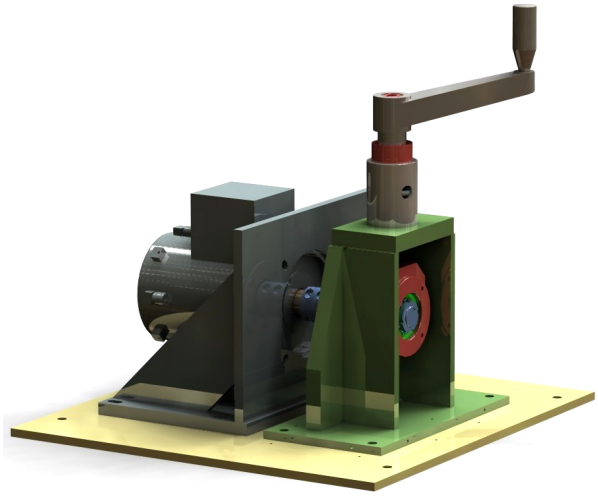

Figure 1. CAD sketch of the test rig

1. INTRODUCTION

In recent researches three different approaches for the diagnosis of bearing faults are widely used for the validation of diagnosis methods. They can be classified as offline faults, when the tested bearings are removed from their in situ position, and online faults, which are generated by means of measures for the accelerated bearing aging.
The authors in (Blödt, Granjon, Raison, & Rostaing, 2008) describe the usage of bearings, which are issued from industrial maintenance, for the verification of their bearing fault modeling. Others like in (Bellini, Immovilli, Rubini, & Tassoni, 2008) examine new bearings which are artificially damaged. They introduce a mechanical load of $40\,\mathrm{kN}$ to simulate brinelling and roughen the surface of the outer ring to produce a single defect on the raceway. Another methode is also the drilling of holes into the raceways of the bearings, which is used in the approach of (Blödt et al., 2008).
In (Stack, Habetler, & Harley, 2005) the problems of both offline approaches are discussed. They state, since the changes

to the probed machine during the removal and mounting of the bearings lead to differing test conditions, the experimental data is corrupted. Thus, to avoid these problems the third approach is to produce an artificially accelerated bearing damage by the application of loads which are higher than the approved design point of the bearing. In (Janjarasjitt, Ocak, & Loparo, 2008) it is described that bearing failure can be generated by a combination of axial load (about $154\,\mathrm{kg}$) and a high operating temperature (about $260\,\mathrm{F}$). The overall lifespan of new bearings are thereby reduced to approximately one month.

Another approach to generate online bearing failures is the application of a current, which flows directly through the test bearing. This method is called fluting and the phenomenon is rarely discovered. The authors in (Boyanton & Hodges, 2002) discuss their observations concerning fluting in case of paper machines. Here, the control unit of the paper machines created a potential on the shaft, which led to electrical discharge machining (EDM) in the bearing. Beside the existence of a potential, whereat about 3 or $4\,\mathrm{V}$ are enough to produce first spark erosions, the appearance of fluting also depends on the lubrication's state, since the oil film around the rolling elements has an insulating effect. When the oil film is thin enough (for example in areas of high load) first spark erosions arise, which generate small pits burned into the races.

Beside the decision between online or offline bearing faults also the selected load influences the diagnostic methods. In addition to the aforementioned fluting, many authors like in (Kim & Parlos, 2002) or in (Raison, Rostaing, Butscher, & Maroni, 2002) concentrate on an applied moment. Mostly, this load is generated by a second electric motor with adjustable torque and speed. Only few authors like in (McFadden & Smith, 1985) choose radial force for online bearing faults, although it is a realistic and common load of a bearing.

The implementation and evaluation of diagnostic and prognostic algorithms demand signal processing and data reduction techniques. (Jardine, Lin, & Banjevic, 2006) suggest different signal processing methods aiming at the extraction of features from the signal, which cover vital information about the motor. The authors distinguish between time domain, frequency domain and time-frequency signal processing methods. Each obtained feature can be sensitive to different fault mode.

One main problem of using multiple feature extraction methods is the resulting high amount of data, which is hard to deal with in case of fault diagnostics (Aye, Heyns, & Thiart, 2014). Thus, the need of data reduction methods arises. One way to identify pattern and transform the data into fewer principal components is the Principal Component Analysis (PCA). The method is widely used with a broad application field like face recognition and data compression, but also for fault detection and classification. For instance (Chirico, Kolodziej, & Hall, 2012) use the PCA for detection and isolation of electro-mechanical actuator faults and (Malhi & Gao, 2004) for a feature selection scheme for a bearing test bed.

The test bench described in the next section provides the application of the two loads for the generation of online bearing faults: Fluting and radial force. After the explanation of the test bed setup, the data reduction and processing part is shortly introduced in section 3. First experimental results of the radial force and fluting concerning the frequency spectrum and the PCA are presented in sections 4 and 5, respectively. The paper ends with a conclusion and a short outlook on upcoming steps.

2. TEST BED SETUP

One main topic of this paper is the description of the test bench, which is used for the generation of run to failure data of bearings. Therefore, the platform with its mechanical parts and the components for the different types of applied loads are presented in the first part. The measurement concept for the data acquisition with the plugged sensors is explained afterwards and the last subsection will be a compilation of the different types of test bearings.

2.1. Mechanical parts and types of applied load

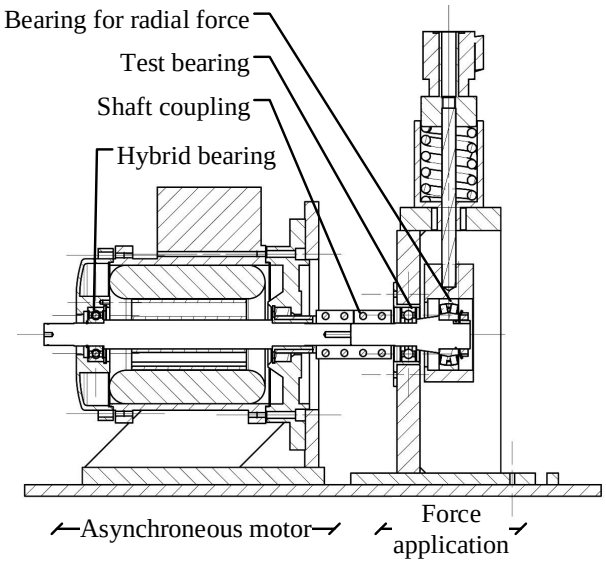

Figure 2. Cross section of the test bench

A cross section of the CAD sketch in Figure 1 is presented in Figure 2. Core piece of the test bench is a simple three-phase a.c. motor of type *80S/2* of the manufacturer *Emod Motoren*. The standard power of this motor is $0.75\,\mathrm{kW}$ at a line to line voltage of $115\,\mathrm{V}$. The supply frequency is $f_s = 50\,\mathrm{Hz}$, it has two terminal pairs and for most of the experiments a slip of $s \cdot f_s \approx 0.3\,\mathrm{Hz}$. The motor is depicted on the left of Figure 2. The power supply is provided by three type *1001SL* of the manufacturer *Elgar*, which enable a variable supply fre-

quency and voltage.
One main change in comparison to the delivery status of the motor is the displacement of the loose bearing (which is also the test bearing) out of the casing into a separate bearing bracket (see right side of Figure 2) for a more time-efficient disassembly. Therefore, the motor shaft is extended by a second shaft, whereat both are connected by a stiff coupling. This ensures that vibrations of the test bearing are directly transmitted to the motor shaft and, thus, are detected by the analysis of the stator current.
Three different types of load are chosen for an artificially accelerated bearing aging: Radial force, fluting of the test bearing and the contamination of the lubrication. The radial force is introduced by a ball joint bearing, which ensures a free angular movement of the shafts. By turning the crank lever (see Figure 1) in combination with a threaded rod and a bearing sleeve, the joint ball bearing is deflected. A spring in the force flow ensures a linear increase of the applied force, which is proportional to the number of revolutions (each revolution corresponds to 140 N). The maximum force that can be provided is 3320 N until the spring runs onto block. Since the distance between test bearing and joint ball bearing is small ($\approx$ 32 mm), the effective load of the test bearing is approximately 3 kN.

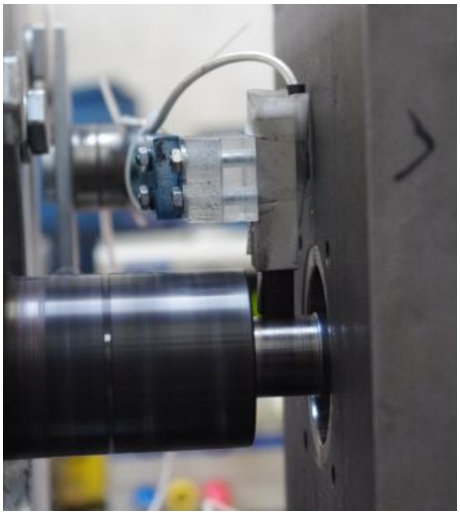

Figure 3. Carbon brush for fluting

Another change to the motor is caused by the application of fluting. As a current is supposed to flow through the test bearing, the motor shaft has to be insulated. Thus, the original fixed bearing of the motor is exchanged by a hybrid bearing to circumvent a current flow through the motor casing. Also the ball joint bearing is in an insulated hull to prevent a flow through this bearing instead of the tested one. As depicted in Figure 3 the current is introduced by a carbon brush, which is pressed on the shaft near the test bearing. To imitate the influences of high frequency switching motor drives, the current is rotary with a supply frequency of 50 Hz and a voltage of up to 9 V. A DSPACE system provides the signal for the voltage, whereat it is amplified by an op-amp (*OPA541* by *Burr-Brown*). The op-amp and the voltage is designed to generate a resulting current through the bearing with a maximum amplitude of about 3 A; a cutout of this signal is plotted in Figure 4. It can be seen that the current shows a hysteresis behavior especially in the voltage area near null. It is assumed that this behavior is caused by the lubrication which varies the overall resistance between the outer and inner ring. Especially in areas of low voltage, the lubrication increases the overall resistance so that the current flow is blocked. Finally, the circuit is closed by connecting the bearing bracket first with a load resistor which prevents a real short-circuit. The load resistor is then connected to the ground of the motor.

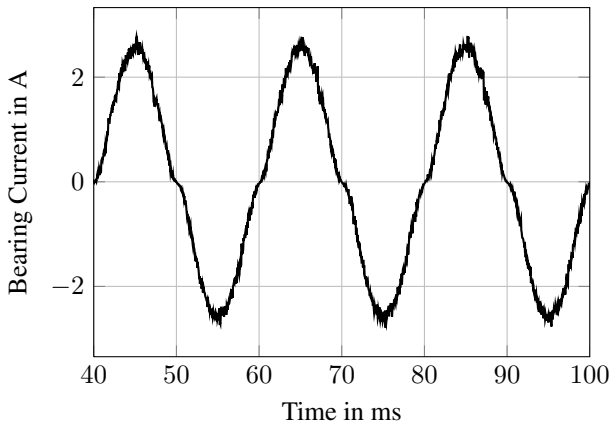

Figure 4. Current through test bearing

On the basis of this test bed the generation of run to failure data in a time duration of few days until several weeks with respect to the applied amount and type of load is possible.

2.2. Data acquisition

The data acquisition system is based on a DSPACE 1103 controller board and a comprehensive sensor suite, which is listed in Table 1. The phase currents of the motor are measured by three closed loop sensors. Another current sensor determines the applied load of the test bearing during a fluting experiment by recording the output of the op-amp.
In order to compare and especially assess the performance of current based diagnostic methods, an accelerometer is mounted on the bearing bracket next to the test bearing in radial direction. The vibration and current signals are sampled with a frequency of 25 kHz, before the signals are filtered by means of a 10 kHz low-pass filter. The ambient and bearing temperature as well as the rotation speed of the shaft are captured once per second. The recording of measurement data is performed every two minutes and lasts 10 seconds.

Table 1. Sensor suite of the test rig

Sensor	Type	Qty	Measurement
Current sensor	LEM LA 25-NP	3	Motor phase
Current sensor	LEM LA 25-NP	1	Fluting current
Accelerometer	Kistler 8702	1	Radial vibration
Temperature sensor	National Semiconductor LM35	2	Bearing and ambient temperature
Position sensor	Honeywell SS495A1	1	Shaft rotation

2.3. Examined bearing types

The test bearing in the bearing bracket is mounted in a hull which can be exchanged. Depending on the diameter D, different types of bearings can be examined. Other differentiating factors are manufacturer, rolling element, dynamic and static load C and C_0, the designation and the price per bearing (exclusive VAT). A small listing of the employed bearings is given in Table 2.

Table 2. Listing of the examined bearings

OEM	D [mm]	Rolling element	C/C_0 [kN]	Type No.	Price [€]
SKF	32	Balls	4.03/ 2.32	61804	8,73
SKF	42	Balls	7.28/ 4.05	16004	5,81
ISB	32	Balls	3.95/ 2.30	61804	2,46
ISB	42	Balls	7.14/ 4.00	16004	2,35
ISB	47	Cylinder	25.00/ 22.00	NU204	8,30

3. DATA PROCESSING AND REDUCTION METHOD

For the evaluation and interpretation of the measured current data a signal processing and reduction method is applied. The applied approach is based on the current signal of one motor phase. The performance of the motor diagnostic depends highly on the extraction of an appropriate feature set. In order to make sure that important information of the motor condition is covered a comprehensive set of features is prepared, which is discussed in section 3.1. As a result each measurement record is transformed into a high dimensional feature vector.

Though the resulting feature vector includes much vital information of the motor, a drawback is that the generated high dimensional vector is not suitable for many data driven diagnostic methods. Hence, the principal component technique is executed in order to map the condition information of the motor in a fewer dimensional vector. Section 3.2 gives a short introduction of this method.

3.1. Signal processing

Given the total amount of N measurements, which are obtained from one experiment, each record n is transferred to a feature vector. The resulting vector is defined as $\mathbf{f}_n = (f_{n1}, f_{n2}, f_{ni}, ..., f_{nI})$, where f_{ni} is the i^{th} feature of overall I characteristic values. In our case all in all 46 features are generated and summarized in the vector. The condition of the motor is described by means of a set of statistical time domain and frequency domain values. The features were taken from the reference (Delgado, Garcia, & Ortega, 2011), where a detailed explanation and the equations of the features can be found.

The statistical information of the temporal signal is determined by six features: Root mean square, peak to peak, standard deviation, crest factor, skewness and kurtosis.

For the frequency domain features the amplitudes of each record's Power Spectral Density (PSD) up to a frequency of 400 Hz is investigated. Higher frequencies are neglected, since fault phenomenons, e.g. characteristic bearing fault frequencies, are expected below this limit (see section 4.1). The relevant frequency range is divided into ten equal bands. The amplitudes within each band are the basis for the calculation of four features: Mean value of the band, standard deviation of the band, skewness and kurtosis of the band. Alltogether 40 features are obtained from the frequency domain.

Finally, all vectors $\mathbf{f}_n$ of an experiment are combined into a $N \times I$ feature matrix $\mathbf{F}$. Since the PCA is very sensitive to outlines, a moving average filter is applied, which smoothes the trend of each feature value over the time.

3.2. Principal Component Analysis

The PCA is a widely accepted technique for data compression and feature extraction. A detailed description of the method including the mathematical equations can be found in (Jolliffe, 2002) or (Alpaydin, 2014).

In general, the PCA is used to transform the feature matrix $\mathbf{F}$ in a new $N \times J$ matrix $\mathbf{G}$. One aim of the method is that $J < I$ is valid without much loss of information. For this purpose correlated variables of the data set $\mathbf{F}$ are combined by the PCA into a set of linearly uncorrelated variables. The PCA identifies the so-called principal components of the feature matrix, which emphasize variation and patterns in the data set. Each feature vector $\mathbf{f}_n$ is mapped to a new vector $\mathbf{g}_n = (g_{n1}, g_{n2}, g_{nj}, ..., g_{nJ})$, where g_{nj} is the j^{th} of a total of J principal components. The transformation is done by the

following equation:

$$\mathbf{g}_{nj} = e_{j1}f_{n1} + e_{j2}f_{n2} + e_{j3}f_{n3} + ... + e_{JI}f_{nI} \quad (1)$$

The coefficients e_{ji} are eigenvector components, which are obtained from the covariance matrix of the feature matrix **F**. Performing the transformation for $j = 1...J$ by using equation 1 gives the principal components in order of significance (highest to lowest). In other words, the first component ($j = 1$) describes the most variance of the training data set, whereas the second component explains the second most variance, and so forth. Hence, the former components give the most insight into a change of the motor condition. On the other hand, discarding the last components in order to reduce the dimension is possible, since the loss of information is insignificant. However, the rate of reduction depends on the data set **F** and the level of variance, which is covered from the remaining components, see section 4.2.

4. EXPERIMENTAL RESULTS WITH RADIAL FORCE

The application of radial force as a load of the tested bearing provides several experimental possibilities, which will be discussed in this section. Most of the trials focus on the generation of run to failure data by means of a variable applied force. The data set which is the basis for the investigations in this section has e.g. five different load states: first state is nearly with no force at the beginning of the trial (corresponds to 16 revolutions of the crank lever; at this point, the spring is still unstressed). The second state is an increased load of about $1680\,N$ or 28 revolutions. In case of the third, forth and fifth state the crank lever is turned once at each time (every revolution introduces an increase of $140\,$N) so that the fifth state corresponds to a load of $2100\,$N and 31 revolutions, respectively.

The results in the next sections are based on the analysis of the stator current signal and its variations due to the radial load only. The mechanism behind these variations can be explained as follows: an increase in the load of the shaft results in a higher displacement of the shaft's rotation axis. Thus, a varying load also leads to a changing air gap in the asynchronous motor which can be detected in the stator current.

The influences of this varying radial force concerning the PSD and the resulting damage cases are presented in a first part. Afterwards, the data reduction to distinguish the single load states by means of the PCA is shown.

4.1. Influences and damage cases

In Figure 5 the PSD spectrum of the current signal during two load changes is depicted over about 1200 measurement cycles, whereat one cycle corresponds to 2 min. For the reduction of noise, the PSD values over the time are low-pass filtered. The first load change is in cycle 420 from about $1680\,$N to $1820\,$N (corresponds to one revolution) and the second change is another turn in cycle 1180 to about $1960\,$N. The corresponding deflection of the shaft inside the motor is about 0.13 mm (about $0.067\,$mm/kN). Although the differences in the deflections are small, they can be detected in the PSD spectrum by comparing the amplitudes of frequency $155\,$Hz ($\equiv 1680\,$N), $162\,$Hz ($\equiv 1820\,$N) and $191\,$Hz ($\equiv 1960\,$N) over the time. Although these frequencies result from a graphical investigation only, it can be seen in Figure 5 that e.g. the amplitudes of frequency $162\,$Hz and $191\,$Hz in the left part of the plot are comparatively small in contrast to those of frequency $155\,$Hz and vice versa. Thus, the amount of load can be spotted by means of the stator current signal.

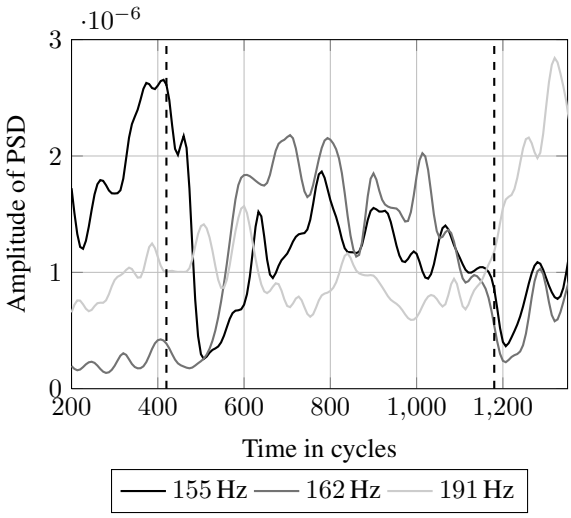

Figure 5. Different levels of load at characteristic frequencies in the PSD spectrum of the stator current (dashed black vertical lines mark the changes in load).

The cases of damage which are produced by a radial force higher than the approved load are mainly broken cages and chattermarks, which are located in the upper half of the outer ring (area of highest load). The corresponding characteristic fault frequencies in the outer raceway, which are presented e.g. in (Blödt et al., 2008), could not be varified during our experiments, since there were no changes in comparison to a healthy bearing.

Although the diagnosis of faulty bearings are in the focus of the investigations, also the failure of the shaft can be detected by analyzing the stator current. One consequence of the high radial load is also a high stress in the shaft which led to a crack in the feather key groove during one of the experiments. Since this fault was not recognized, the crack grew over several hours, which is depicted by means of the PSD spectrum in Figure 6. The exponential behavior of the amplitudes is clearly visible which is characteristic for a crack growth concerning assumptions like the Paris law. However, it must be mentioned that the data base for a certain statement about the cause of damage is too small so that the depicted rise of the amplitudes can also refer to a bearing fault.

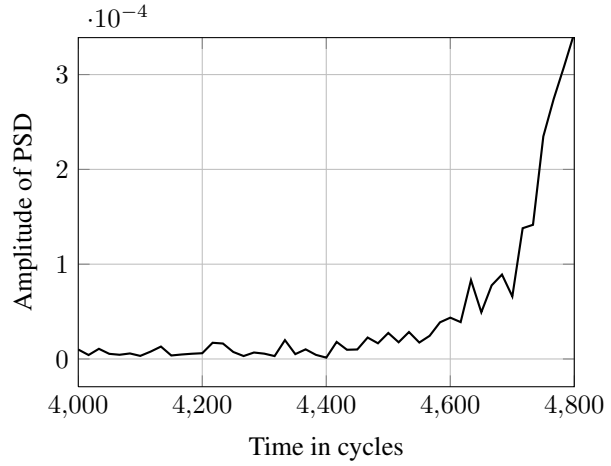

Figure 6. PSD values of the stator current at a frequency of 212 Hz over the last cycles before the shaft breaks down

4.2. Determination of load conditions using PCA

In this section the focus is on the distinction between the load conditions applying the data processing and reduction method, described in section 3. Therefore 100 records of the current signal for each five load conditions are used to generate a 46×500 feature matrix **F**. By means of the reduction method the feature matrix is transformed into a 3×500 matrix **G**. The remaining components cover about 94 percent of the variance of the original data set. This means, instead of 46 features only the first three principal components are used for the load determination. The data of the resulting matrix is illustrated in Figure 7.

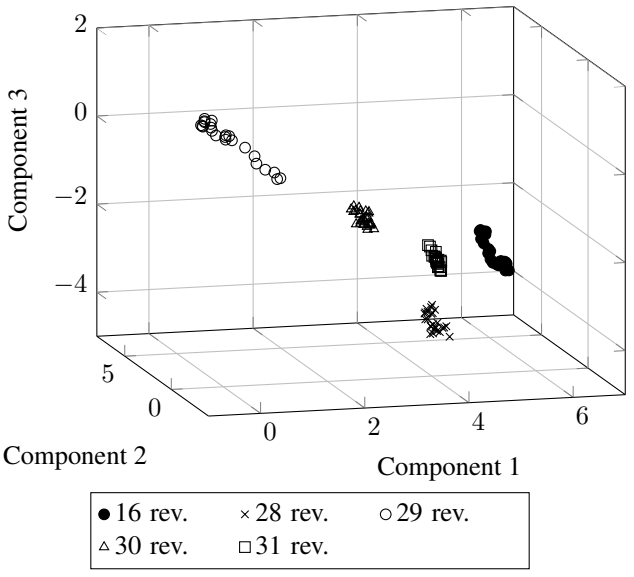

Figure 7. The first three principal components of the data set using five different radial forces as a load of the tested bearing

It is evident that the resulting data is clustered according to the load conditions. Thus, investigating the first three principal components of the data makes an easy distinction possible.
In a next step the reduced feature matrix **G** and the corresponding eigenvectors could be used as training data for a data driven classification of different load conditions. Thus, this trained classifier could distinguish between different load levels in case of new test data.

5. EXPERIMENTAL RESULTS WITH FLUTING

The influences of fluting on the degradation of a bearing is rarely discovered as mentioned in section 1. Especially a convenient magnitude of the applied current through the bearing is hardly discussed or the recommended values vary in recent researches.
Similarly to section 4 the influences of fluting on the frequency spectrum of the current signal and the generated cases of damage are presented first. An approach for the extraction of a health indicator representing the current state of the bearing by means of the PCA is described afterwards. Since the application of fluting in this test bench is new, only three run to failure data sets are available for the comparison.

5.1. Influences and damage cases

One of the main challenges for the application of fluting is to provide a voltage so that a current flow through the bearing is possible. This aim is complicated, since the resistance between the outer and the inner ring of the bearing varies strongly, as discussed in section 2.1. Especially at the beginning of a new run to failure test this phenomenon can lead to a delayed start of the current flow, since the lubrication of a new bearing insulated the rolling elements from the outer and inner ring. Consequently, the current is too small for the existence of EDM. After a certain period of time (between hours and approximately one day) it is assumed that the thickness of lubrication decreases so that EDM is possible and the current begins to flow through the test bearing.
The beginning of a new test is depicted in Figure 8. Beside the measured bearing current given as the effective value also the PSD values at a frequency of 28 Hz is plotted, since the beginning of the current flow is also visible in the frequency range of the stator current in measure cycle 40. One explanation for this might be that a first EDM produces a pitting in the outer or inner ring of the bearing which leads to a displacement of the shaft's rotation axis. Thus, this movement of the shaft can be detected by the analysis of the stator current signal. Another reason could be that a small current flow through the shaft and the hybrid bearing directly corrupts the stator current.
The PSD spectra of three different instants of time during a life cycle of a bearing are pictured in Figure 9. It is obvious that especially the amplitudes in the frequency domain

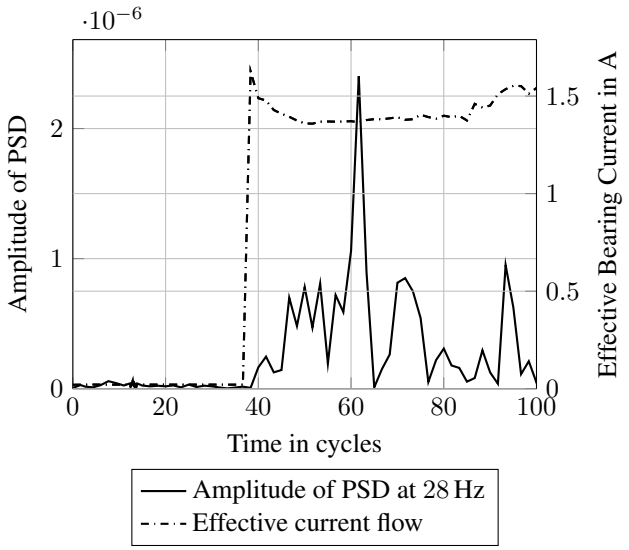

Figure 8. The beginning of fluting both in measured bearing current signal (right axis) and the PSD analysis of the stator current signal of the motor (left axis)

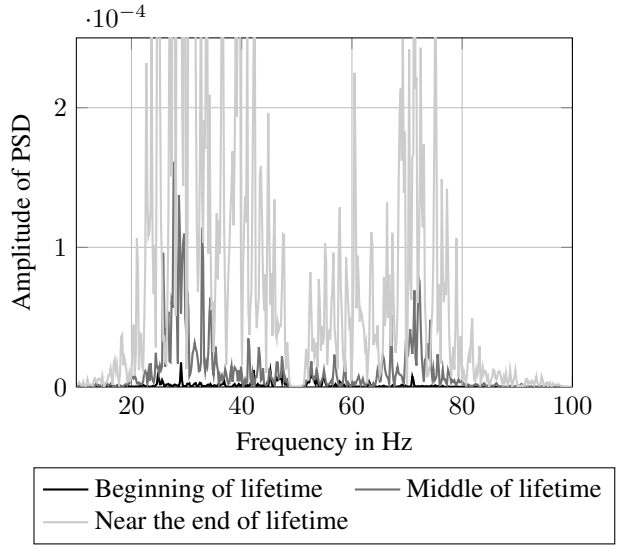

Figure 9. Different states of damage due to fluting represented by the PSD spectra of the stator current signal.

between 20 and 50 Hz increase with proceeding degradation of the bearing. It is important to mention that the supply frequency of 50 Hz is notch filtered and the frequency domain between 50 and 80 Hz is the result of mirroring the aforementioned frequency domain at the supply frequency.
A cross section of all PSD spectra over the time at a frequency of 29 Hz is depicted in Figure 10. The failure mode during this trial was a broken cage, which led to a nearly instant breakdown of the bearing at the end of its life cycle, although the slightly increased amplitudes in the middle of the lifetime is also visible. The overall lifetime was about two days.
The damage which is produced by fluting is material removal.

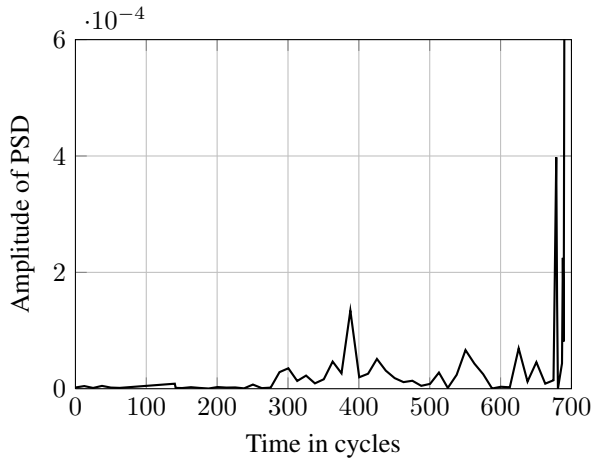

Figure 10. Run to failure data set represented by the PSD amplitudes of the stator current at a frequency of 29 Hz. The failure was created by fluting with an voltage of approximately 9 V.

(a)

(b)

Figure 11. (a) Completely deformed bearing cage (b) Partly bent cage on the right of the picture

Thus, a broken cage and an increased clearance of the bearing are consequences, whereat the latter leads to a direct contact

of the rotor and the stator. In case of a broken cage, two different failure modes could be observed as depicted in Figure 11a and Figure 11b. In Figure 11a the cage is completely deformed and quarried out. In Figure 11b only one link (on the right of the picture) is bent, which sticks the bearing. Both led to a nearly abrupt failure of the bearing.

5.2. Extraction of a health indicator using PCA

Since the PCA is suitable to highlight variance of the determined features over the time (see section 4.2), the described method is applied to extract a health indicator from the current signal of the first three measured run to failure data sets. For this purpose, the first data set is selected as training data, which is used to determine the eigenvalue coefficients of the transformation Equation 1. According to the resulting coefficients, the first three principal components are determined of the three run to failure data sets.
The first principal components of the three experiments are shown in Figure 12. The last 22 hours are displayed before the failure of the bearing occurred. It can be ascertained that all three courses differ strongly and no clear tendency of the bearing's degradation is visible. Furthermore, the final failure limit is located on different values. Thus, the first principal component is not suitable as a health indicator for the motor. Since the other components reveal a similar behavior a presentation is neglected at this point.

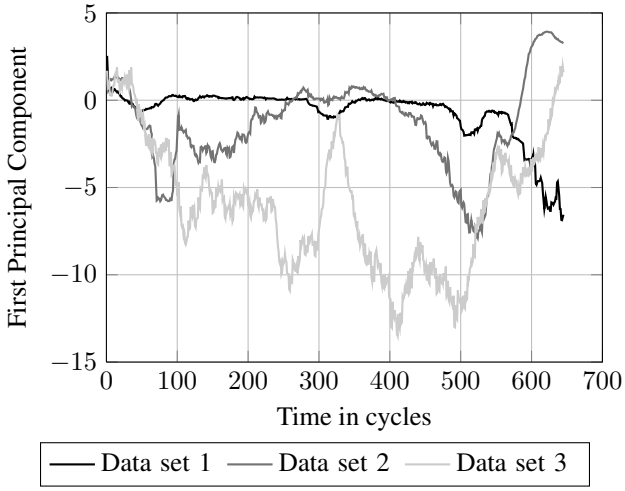

Figure 12. Trend of the first principal component of three run to failure experiments

Another approach to generate a health indicator is to determine the euclidean distance of the first three principal components:

$$G_n = \sqrt{g_{n1}^2 + g_{n2}^2 + g_{n3}^2}. \quad (2)$$

The result is illustrated in Figure 13 which reveals the identical phenomenon of an oscillating trend. A benefit of the generated trends can be seen in a similar failure limit. However, two features cross the limit several times without a failure of the bearing. Thus, a prediction of a failure would be highly unlikely using the combined feature as a health indicator.

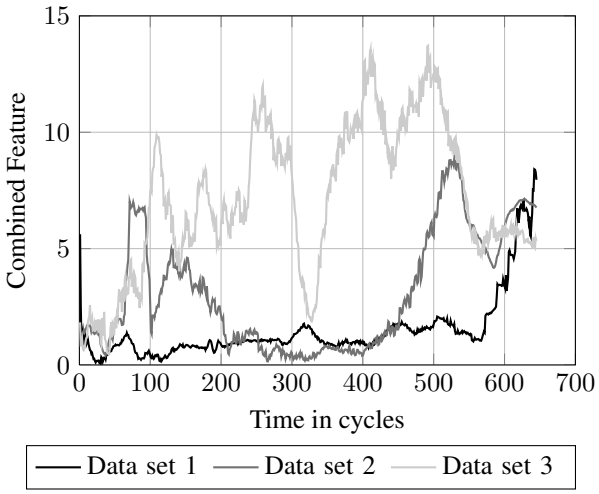

Figure 13. Combined features (based on the first three principal components) of three run to failure experiments

For the purpose of comparing vibration and the current data Figure 14 shows the root mean square values of the corresponding vibration signals. A roughly exponential degradation trend is visible. However, the variation of the final failure limit also hinders a precise prediction of the remaining useful lifetime of the motor.

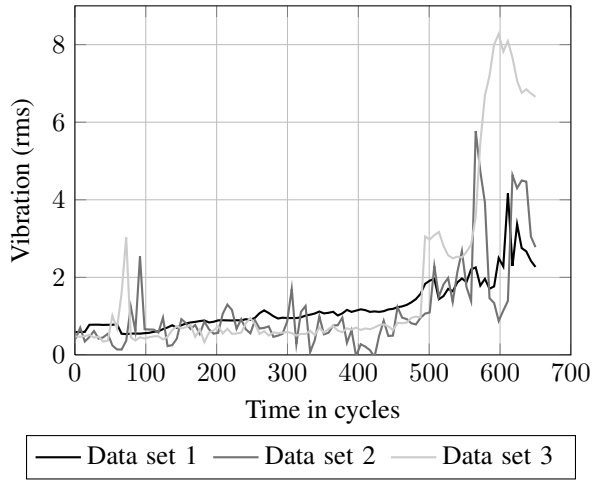

Figure 14. Root mean square values of the vibration signals of three run to failure experiments

6. CONCLUSION

The first diagnostic experimental results of a new test bench were presented in this paper. The focus of this paper was the

illustration of the test bed setup and here especially the components for the application of fluting and radial force. The influences of these loads concerning the frequency spectrum and the achieved bearing failures were discussed, whereat both can be roughly detected by analyzing the PSD of the stator current.

First examinations of theses current signals were done by means of common methods for the post-processing step. The applied data reduction and processing method was tested both for the classification of the applied radial force and for the identification of a health indicator in case of fluting. The PCA was used to find only those features which correspond to the current radial force or the effective health indicator. A data-based classifier trained with these features could distinguish between different states in case of new test data. The classification of the different load levels were successful and especially in comparison to the graphical analysis of the PSD spectra more distinct. The extraction of a health indicator by means of the PCA was more challenging and needs more data sets for better results. The large variance concerning the causes of damage in particular complicates this method.

In the future, it is planned to extend the platform for the radial force by a step motor for an automatic application of predefined loads so that the crank lever will be replaced. Another challenge is the investigation of both combined loads, i.e. fluting and radial force, concerning the lifespan of a bearing. It is expected that this combination reduces the life cycle dramatically, since the insulating effect of the lubrication will decrease especially in the areas of high radial load. Another main issue of the current setting is the high number of broken cages. Since this case of damage occurs abruptly, the extraction of degradation courses is challenging. Thus, the generation of pittings in the raceways or on the rolling elements, which then can be analyzed by means of the familiar characteristic fault frequencies, is one main topic.

When the test bench is completed with all the planned changes, the superior goal will be to generate a data basis for the evaluation of prognosis and diagnosis algorithms to estimate the remaining useful lifetime of bearings by using the current data only.

NOMENCLATURE

C	Dynamic bearing load
C_0	Static bearing load
D	Diameter of the outer ring
$\mathbf{F}$	Feature matrix of an experiment
$\mathbf{f}_n$	Feature vector of record n
f_s	Supply frequency
$\mathbf{G}$	Reduced feature matrix of an experiment
$\mathbf{g}_n$	Reduced feature vector of record n
I	Total number of features
J	Total number of principal components
N	Total number of measurement records
n	Number of a record
s	Slip
EDM	Electrical Discharge Machining
PCA	Principal Component Analysis
PSD	Power Spectral Density

REFERENCES

Alpaydin, E. (2014). *Introduction to machine learning* (Third edition ed.).

Aye, S. A., Heyns, P. S., & Thiart, C. J. (2014). A review of slow speed bearing diagnostics and prognostics. In *International journal of engineering science and technology* (Vol. Vol. 6 No.10, pp. 726–739).

Bellini, A., Immovilli, F., Rubini, R., & Tassoni, C. (2008). Diagnosis of Bearing Faults in Induction Machines by Vibration or Current Signals: A Critical Comparison. *Industry Applications Society Annual Meeting, 2008. IAS'08. IEEE*(46), 1–8.

Blödt, M., Granjon, P., Raison, B., & Rostaing, G. (2008). Models for Bearing Damage Detection in Induction Motors Using Stator Current Monitoring. *IEEE Transactions on Industrial Electronics*, *55*(4), 1813–1822. doi: 10.1109/TIE.2008.917108

Boyanton, H. E., & Hodges, G. (2002). Bearing fluting: the results of a long-term investigation into bearing fluting on AC motors, DC motors, and Rolls on paper machines. *IEEE Industry Applications Magazine*, *2002*(Sep/Oct issue), 53–57.

Chirico, A. J., Kolodziej, J. R., & Hall, L. (2012). A data driven frequency based feature extraction and classification method for ema fault detection and isolation. In *Asme 2012 5th annual dynamic systems and control conference joint with the jsme 2012 11th motion and vibration conference* (pp. 751–760).

Delgado, M., Garcia, A., & Ortega, J. A. (2011). Evaluation of feature calculation methods for electromechanical system diagnosis. In *8th ieee international symposium on diagnostics for electric machines, power electronics and drives - (sdemped 2011)* (pp. 495–502). doi: 10.1109/DEMPED.2011.6063669

Janjarasjitt, S., Ocak, H., & Loparo, K. (2008). Bearing condition diagnosis and prognosis using applied nonlinear dynamical analysis of machine vibration signal. *Journal of Sound and Vibration*, *317*(1-2), 112–126. doi: 10.1016/j.jsv.2008.02.051

Jardine, A. K., Lin, D., & Banjevic, D. (2006). A review on machinery diagnostics and prognostics implementing condition-based maintenance. *Mechanical Systems and Signal Processing*, *20*(7), 1483–1510. doi: 10.1016/j.ymssp.2005.09.012

Jolliffe, I. T. (2002). *Principal component analysis* (2nd ed ed.). New York: Springer.

Kim, & Parlos. (2002). Induction motor fault diagnosis based on neuropredictors and wavelet signal processing - Mechatronics, IEEE/ASME Transactions on. *IEEE Transactions on Industrial Electronics*.

Malhi, A., & Gao, R. X. (2004). Pca-based feature selection scheme for machine defect classification. *IEEE Transactions on Instrumentation and Measurement*, *53*(6), 1517–1525. doi: 10.1109/TIM.2004.834070

McFadden, P. D., & Smith, J. D. (1985). The vibration produced by multiple point defects in a rolling element bearing. *Journal of Sound and Vibration*, *98*(2), 263–273. doi: 10.1016/0022-460X(85)90390-6

Raison, B., Rostaing, G., Butscher, O., & Maroni, C.-S. (2002). Investigations of algorithms for bearing fault detection in induction drives - Industrial Elelctronics Society, IEEE 2002 28th Annual Conference of the. *IECON 02 [Industrial Electronics Society, IEEE 2002 28th Annual Conference of the] (Volume:2)*(2), 1696–1701.

Stack, J. R., Habetler, T. G., & Harley, R. G. (2005). Experimentally Generating Faults in Rolling Element Bearings Via Shaft Current. *IEEE Transactions on Industry Applications*, *41*(1), 25–29. doi: 10.1109/TIA.2004.840966